Radiography of Soft Tissue of the Foot and Ankle with Diffraction Enhanced Imaging

Jun Li*
Zhong Zhong†
Roy Lidtke‡
Klaus E. Kuettner*
Charles Peterfy§
Elmira Aliyeva*
Carol Muehleman||

Non-calcified tissues, including tendons, ligaments, adipose tissue and cartilage, are not visible, for any practical purposes, with conventional X-ray imaging. Therefore, any pathological changes in these tissues generally necessitate detection through magnetic resonance imaging or ultrasound technology. Until recently the development of an X-ray imaging technique that could detect both bone and soft tissues seemed unrealistic. However, the introduction of diffraction enhanced X-ray imaging (DEI) which is capable of rendering images with absorption, refraction and scatter rejection qualities has allowed detection of specific soft tissues based on small differences in tissue densities. Here we show for the first time that DEI allows high contrast imaging of soft tissues, including ligaments, tendons and adipose tissue, of the human foot and ankle. (J Am Podiatr Med Assoc 94(3): 315-322, 2004)

Introduction

Historically, soft tissues of the body such as muscle, ligaments, tendons and cartilage have been imaged by techniques other than conventional radiography, such as magnetic resonance imaging (MRI) and ultrasound. Because of their relatively low tissue densities, soft tissues have low X-ray absorptive ability and therefore generally appear as mere shadows in a conventional radiograph of a body region (Staren, 1980). However, a novel X-ray technology, called diffraction enhanced imaging (DEI), carried out at the National Synchrotron Light Source (NSLS) at Brookhaven National Laboratory, has previously been shown to allow visualization of breast tissue (Chapman et al. 1998) and articular cartilage of

*Department of Biochemistry, Rush Medical College, Chicago, IL.

†National Synchrotron Light Source, Brookhaven National Laboratory, Upton, NY.

‡Dr. William M. Scholl College of Podiatric Medicine at Finch University and Chicago Medical School, North Chicago, IL.

§SYNARC, Inc, San Francisco, CA.

||Departments of Biochemistry and Anatomy, Rush Medical College, Chicago, IL.

Corresponding author: Carol Muehleman, PhD, Department of Anatomy, Rush Medical College, ACFAC507, 600 S Paulina, Chicago, IL 60612.

From *Journal of Anatomy* **202:** 463–470, 2003. Reprinted by permission. ©Anatomical Society of Great Britain and Ireland 2003.

human knee joints and the talus of the ankle joint (Mollenhauer et al. 2002).

DEI uses a synchrotron X-ray source because of its highly collimated X-ray beam (Chapman et al. 1997; Zhong et al. 2000) for which there is currently no clinical device of comparable intensity and character. The strength of the technology is that it utilizes a series of perfect silicon crystals to provide images with enhanced contrast depending on the extent of X-ray ultra-small-angle scattering and refraction by the object.

Our intention is not to compare DEI technology with other imaging techniques, such as MRI, ultrasound, and computerized tomographic (CT) scanning, but rather to demonstrate the hitherto undiscovered capabilities of radiography for soft tissue imaging. Until recently, it was thought that radiography had reached an endpoint in terms of imaging for medical purposes.

Here we describe for the first time the X-ray imaging, through DEI, of soft tissues, i.e. skin, tendon, ligament, adipose tissue and articular cartilage of the human foot.

Materials and Methods

The DEI System

The details of DEI technology have been presented previously (Chapman et al. 1997; Zhong, 2000; Mollenhauer et al. 2002), and we provide here only a brief description. A schematic of the DEI system used for our experimentation at the XI5A beamline at the NSLS is shown in Fig. 1. The collimated fan beam of X-rays is prepared by the silicon [3,3,3] monochromator consisting of two perfect silicon crystals. Once this beam passes through the subject, a third crystal (analyser crystal) of the same reflection index diffracts the X-rays onto radiographic film (Kodak Professional Industrie 150, Industrex SR45) or an image plate detector (Fuji HRV image plate, readout by a Fuji BAS2500 image-plate reader). The distance between the X-ray source and the specimen is approximately 20 m while the distance between the specimen and the X-ray film or image plate detector is 1 m. The image of the subject is formed by scanning the subject and X-ray film at the same speed through the fan beam, in approximately opposite directions to take account of the Bragg reflection by the analyser crystal. Because of the non-dispersive nature of the crystals, the narrow Darwin-width of the diffraction used, and the small distance between the sample and detector, the resolution of the image obtained is limited by the resolution of the X-ray film, which is approximately 50 μm, or the pixel size of the image plate detector, which is approximately 75 μm.

The Bragg condition for the analyser crystal is met only when the incident beam makes the correct angle with the lattice planes in the crystal for a given X-ray energy. When this condition is met, the beam diffracts from the planes over a narrow range of incident angles. As the analyser crystal is rotated about a horizontal plane, the crystal will go through the Bragg condition for diffraction and the diffracted intensity will trace out a profile or 'rocking curve' (Zachariasen, 1945). The rocking curve of the analyser in the protocol described here is roughly triangular and has a peak intensity close to that of the beam striking it. The width of this profile is typically a few microradians (the full width at half maximum is 1.5 microradians at an X-ray energy of 40 keV and 3.6 microradians at 18 keV, using the Si [3,3,3] reflection). This narrow angular width provides the tools necessary to prepare and analyse, on the microradian scale, the angle of X-ray beams modified by the subject while traversing it. Since the range of angles

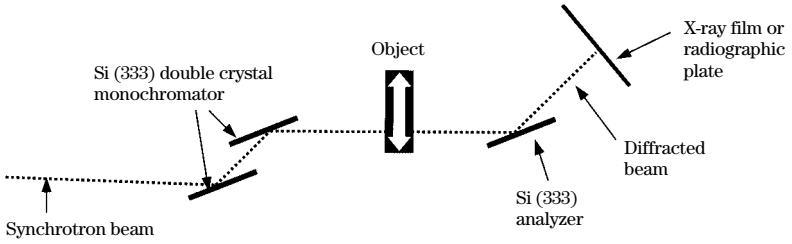


Figure 1. Schematic representation of the DEI set-up at the NSLS synchrotron. The synchrotron beam, whose energy level is selected by the Si (3,3,3) double crystal monochromator, passes through the object and subsequently through a matching Si (3,3,3) analyser crystal that is located between the object and the detector. The high-resolution X-ray film and the radiographic image plate were used as the detectors. The beam from the synchrotron is a fan beam, 120 mm wide and 3 mm high, that extends into and out of the plane of the paper. The object and the detector are scanned perpendicular to the beams to create a planar image.

that can be accepted by the analyser crystal is only a few microradians, the analyser crystal detects the subject's X-ray scattering (ultra-small-angle scattering) and refraction of X-rays at the microradian level, an angular sensitivity which is not possible in conventional radiography. The X-ray intensity in the subject image is therefore modulated by the scattering and refraction properties of the subject. To extract refraction information, the analyser is typically set to the half intensity points on the low- and high-angle sides of the rocking curve (referred to as –1 and +1, respectively, in the following discussion), or at the base of the rocking curve (referred to as –2 and +2, respectively, for the low- and high-angle sides), while the imaging takes place. For optimal extinction (scatter rejection) sensitivity, the analyser is typically set to the peak of the rocking curve during imaging.

The reproducibility of the DE images is maintained by monitoring the intensity of the diffracted X-rays by the analyser just prior to imaging to ensure that the analyser is at the prescribed angular position.

Specimens

The study sample consisted of one fresh-frozen great toe separated from the foot at the cuneiform–first metatarsal joint and a complete human foot along with three great toes preserved in 10% formalin. All specimens were procured from a surgical workshop through the courtesy of Ortheon Medical (Winter Park, FL, USA). Just prior to imaging, the fresh-frozen toe was allowed to defrost at room temperature.

Imaging

All specimens were imaged in a medial to lateral direction and at 40 keV with DEI, and by 'conventional' synchrotron X-ray radiography by removing the analyser crystal and scanning the subject and detector through the monochromatic fan beam, at the same X-ray energy using the same X-ray dose as DEI. It should be noted that a 'conventional' synchrotron X-ray image is of high quality in comparison to a non-synchrotron radiograph. Depending on the current of the electron storage ring, the skin dose delivered was measured with an ion chamber and maintained by adjusting the speed of each scan.

When using the image plates as the detector, the dose delivered to the specimen was 0.12 milli-gray per image, over an exposure time of approximately 30 s to cover an imaging area of 30 mm by 120 mm. This dose is well below the typical dose of 0.2 milli-gray with screen-film or digital systems, used for diagnostic X-rays of the extremities. In an effort to achieve highest possible resolution, phosphor screens were not used with the films, resulting in low efficiency of the high-resolution films at 40 keV. Thus, with films as the detector, the dose delivered was 2.40 milli-gray per image over an exposure time of approximately 10 min.

Each specimen was imaged at least twice by the same synchrotron scientist (Z.Z.) using identical energy and rocking curve parameters to establish reproducibility.

Results

The conventional radiograph and DE image (at +1 of the rocking curve), in lateral view, of an intact first metatarsal and great toe are shown in Fig. 2 A and B, respectively. In the radiograph (Fig. 2A), the bones appear quite osteoporotic. Chondrocalcinosis of the head of the metatarsal within the first metatarsophalangeal joint and a calcified blood vessel are apparent. Except for the faint 'shadow' of the surrounding soft tissues and calcification within a tendon, no other structures are visible. However, the DE image of the same specimen in the same position (Fig. 2B) clearly shows skin, the fat pad beneath the head of the first metatarsal and proximal phalanx, the same sclerotic blood vessel identified in the radiograph, the nail plate and some tendons. Within the fat pad, even the organizational architecture rendered by its collagen framework is apparent.

On the dorsal side of the first metatarsal and proximal phalanx, the tendon of the extensor hallucis longus muscle can be delineated from the surrounding connective tissue and skin. The tendon of the flexor hallucis longus muscle can be seen along the deep plantar aspect, particularly between the sesamoid bones and the proximal phalanx. On the plantar aspect of the metatarsal, the region of the short flexor and adductor hallucis muscles is identifiable.

Figure 3 is a DE image (at +2 of the rocking curve) of the ankle and rear foot that is externally rotated and inverted approximately 15° and slightly dorsiflexed so that the medial aspect of the foot lies superior to the lateral aspect. This view demonstrates the tendons of the tibialis anterior and extensor hallucis longus muscles on the dorsal aspect, beneath the skin and subcutaneous connective tissue. Posterior to the tibia and talus, and deep to the Achilles tendon, is a bundle of tendons, the most prominent of which is that of the fibularis longus. This tendon can be seen passing beneath the lateral malleolus of the fibula, through the superimposed calcaneus bone and beneath the calcaneocuboid joint within the

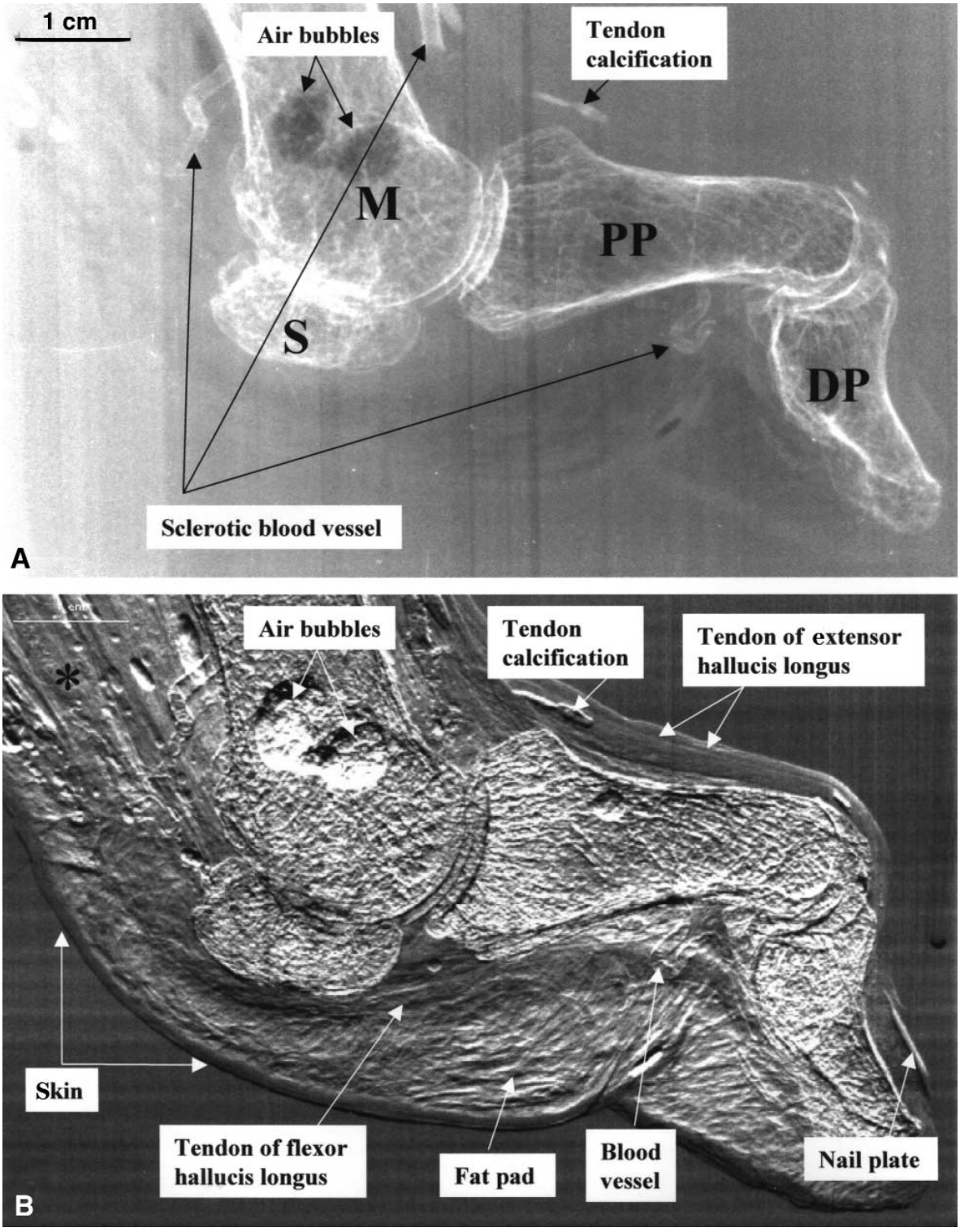


Figure 2. A, Conventional synchrotron radiograph of the great toe that includes the distal portion of the first metatarsal (M), the sesamoid bones (S), the proximal phalanx (PP) and the distal phalanx (DP). The osteoporotic bones are evident as are the sclerotic vessels. B, DE image of the same specimen as in part A taken at +1 of the rocking curve. The major soft tissue structures that can be identified here, which are not visible in the above radiograph, include the two major tendons of the toe, the fat pad under the ball of the foot (which has been displaced distally somewhat) and the skin. The asterisk indicates the location of the muscles and tendons plantar to the first metatarsal bone. These cannot be delineated from one another in this image.

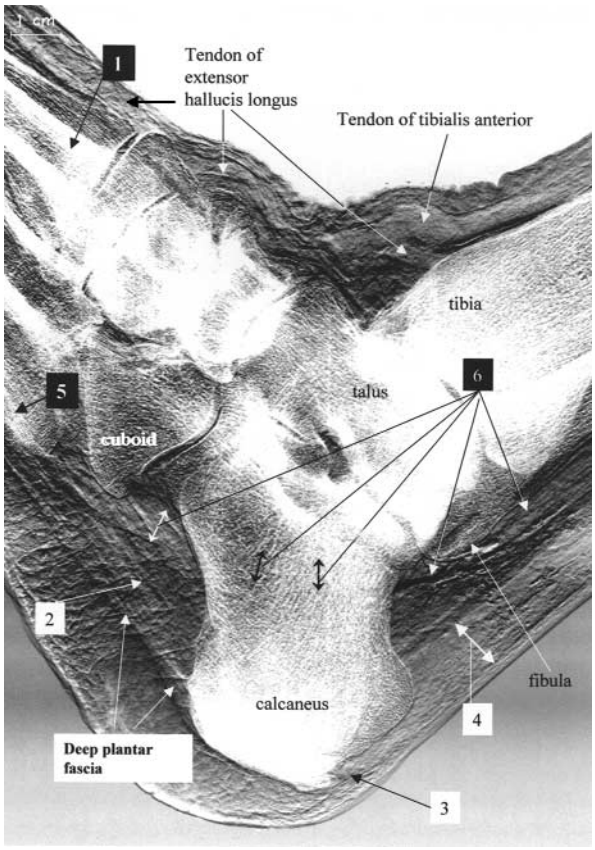


Figure 3. DE image taken at +2 of the rocking curve showing the bones and soft tissues of the ankle and proximal foot of a right lower extremity. Two dorsal tendons are apparent. Labelled structures are: 1, first metatarsal bone; 2, intrinsic muscles of the plantar aspect of the foot; 3, distal attachment of the Achilles tendon on the calcaneus; 4, body of the Achilles tendon; 5, fifth metatarsal bone; and 6, tendons and muscles lying posterior to the tibia and fibula, the most prominent of which is the fibularis longus whose tendon can be seen passing behind the lateral malleolus of the fibula, through the superimposed calcaneus and beneath the calcaneocuboid joint.

plantar foot. The insertion of the Achilles tendon at the posterior aspect of the calcaneus is seen. The deep plantar fascia can also be observed as a band running distally from the calcaneus, lying between the intrinsic muscles of the plantar foot and the superficial fascia.

The intrinsic muscles of the plantar foot can only be seen as a mass of tissue without delineation between individual components. Only the outline of the tendon of the fibularis longus muscle can be discriminated due to the refraction change between tissues of different densities.

Figure 4A is a conventional radiograph of the first metatarsophalangeal joint positioned so that a portion of the joint space was visible for the identification of articular cartilage. Only the calcified components of the joint are visible. The DE image of the same specimen taken at –1 of the rocking curve is seen in Fig. 4B. The articular cartilage of the first metatarsal and of the proximal phalanx are seen, as are the joint capsule and ligaments. It may also be noted that the architecture of the bone tissue has a more three-dimensional appearance due to the ability of DEI to capture refraction information, particularly at the –1 and +1 positions of the rocking curve. A higher magnification of the DE image of the same specimen taken with the analyser at three different positions (–1, peak, and +1) of the rocking curve is shown in Fig. 5 to demonstrate the different appearance of the tissues when the position of the analyser is changed. It is noteworthy that the boundary of the cartilage of the metatarsal can also be followed even through its superimposition by the proximal phalanx. The images off the peak of the rocking curve provide the best delineation of the boundaries of the articular cartilage owing to the refractive effects at these points.

Discussion

The goal of the present study was a preliminary exploration into the ability of the novel X-ray imaging technology, called DEI, to allow visualization of soft tissues of varying densities in the human foot. Previous reports exploring the biological application of DEI have shown that it allows visualization of breast tissue pathologies (Chapman et al. 1998) and the articular cartilage of human knee and ankle joints (Mollenhauer et al. 2002) as well as of rabbit knee joints (Muehleman et al. 2002). Here we show that the skin, ligaments, tendons, the adipose pads with their associated collagenous framework, and an occasional large blood vessel can be delineated with DEI without the aid of a contrast agent. In addition, the articular cartilage of the first metatarsophalangeal joint, a small joint with much thinner cartilage as compared to the knee and ankle joints, was visualized. Certainly, with varying rotations of the anatomical region, different soft tissue structures would be observed. Although some of our images were collected on specimens that were formalin preserved, we previously reported that no differences could be discerned between fresh and preserved specimens (Mollenhauer et al. 2002).

Because of their low contrast characteristics, soft tissues are not visible to any extent with conventional X-rays. A radiographic technique that could provide all of the information that is imparted through

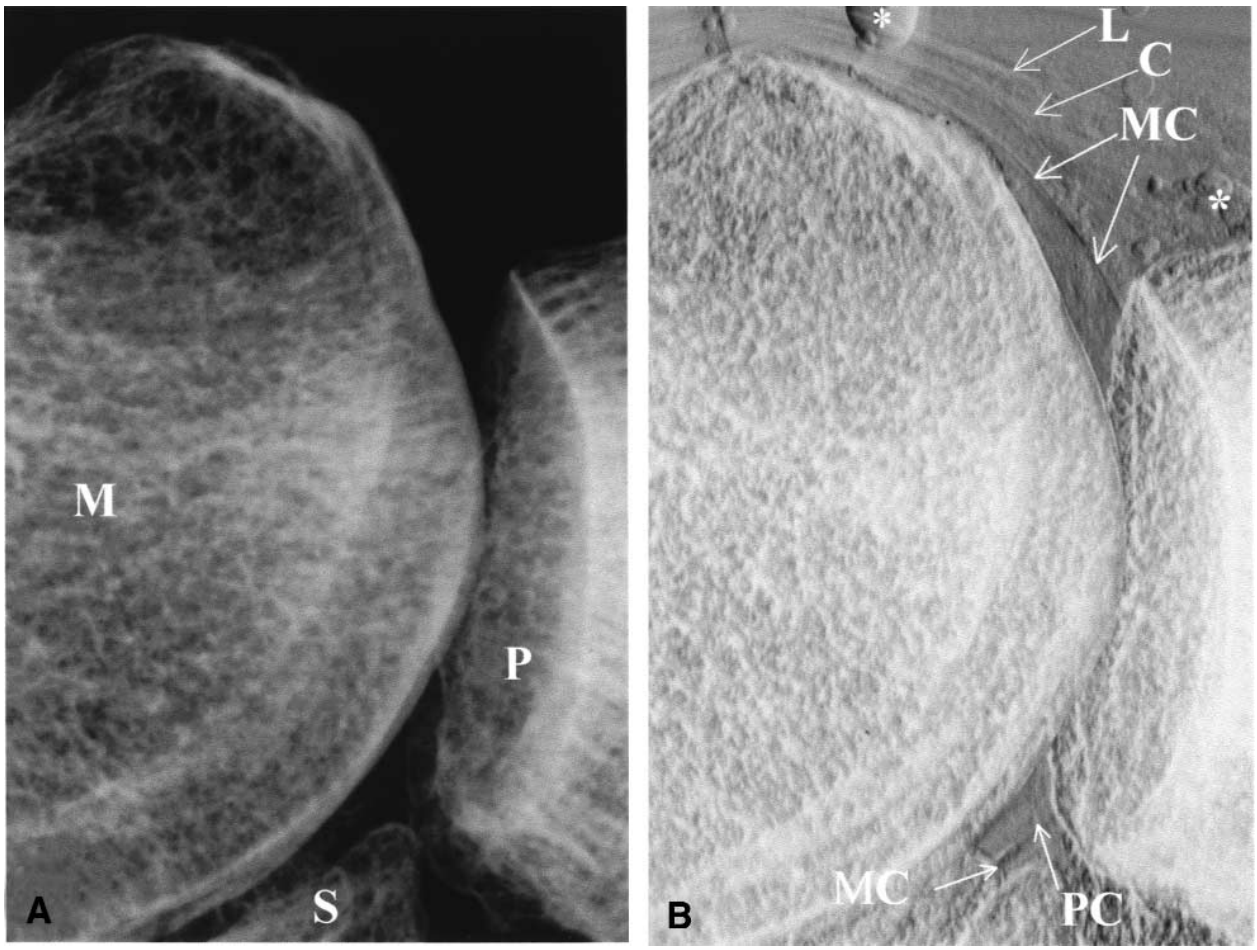


Figure 4. A, Conventional synchrotron radiograph of the first metatarsophalangeal joint showing that only the bony components of the joint are visible: M, head of first metatarsal; S, sesamoid bone; P, base of proximal phalanx. B, DE image of the same specimen at –1 of the rocking curve. Both articular cartilage and the surrounding connective tissue are visible. L, ligament between the head of the first metatarsal bone and base of the first proximal phalanx; C, capsule of the first metatarsophalangeal joint; MC, articular cartilage of the metatarsal; and PC, articular cartilage of the proximal phalanx. Note that the trabecular bone has taken on a three-dimensional appearance. This results from the combination of the refraction information with absorption and scatter-rejection information. Air bubbles are identified by an asterisk.

conventional radiography, with additional information on soft tissue, may prove to be of clinical importance particularly in the detection of soft tissue pathologies.

The non-invasive imaging of both humans and animals for the detection of pathologies, or to follow the efficacy of drug treatments, is of vital importance. Because DEI is based on tissue contrast resulting from differences in tissue densities (refraction contrast) and the organization of the tissue (scatter rejection contrast), X-rays will delineate structures on a completely different basis than will MRI or ultrasound. Thus DEI, which extrapolates upon this principle by providing a high level of resolution and the additional characteristics of refraction and scatter rejection, should be capable of detecting tissue characteristics that differ from those detected by other imaging modalities.

In the present study we have shown that connective tissues, tendons and ligaments can be visualized with X-rays due to the ability of DEI to delineate tissues of similar densities. This is accomplished because DEI harnesses information provided by small-angle scattering within a range accepted by a perfect silicon analyser crystal located between the specimen and the detector. In addition, this analyser crystal can be positioned on different angular settings, thus providing different sensitivity on tissues and

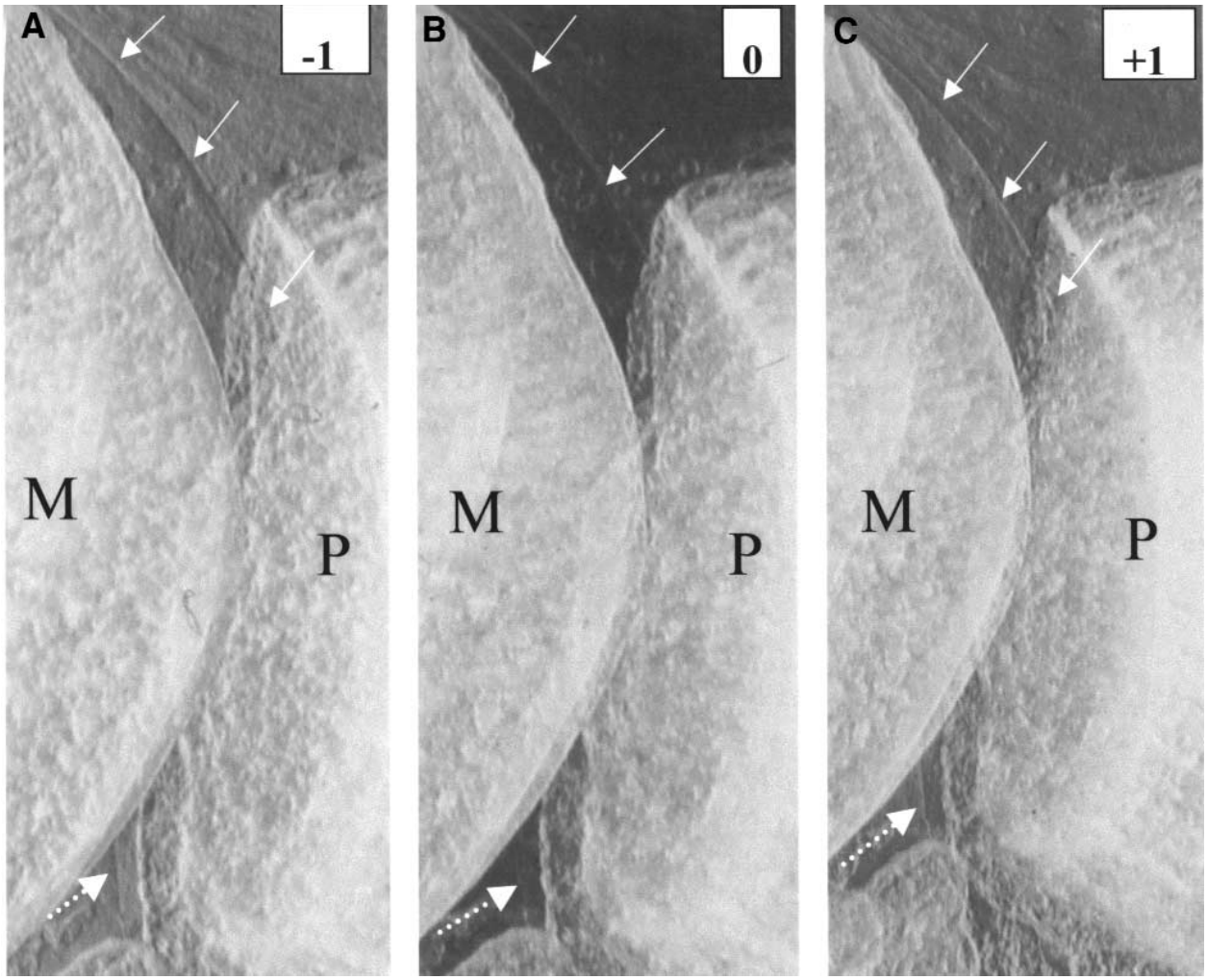


Figure 5. Enlarged DE images of the first metatarsophalangeal joint demonstrating how the character of the image changes at –1, the peak, and +1, respectively, of the rocking curve. M, head of first metatarsal; P, base of proximal phalanx. Note that the shadows have the opposite contrast in the –1 and +1 images. The solid arrows point to the outer boundary of the articular cartilage of the metatarsal while the interrupted arrows point to the outer boundary of the cartilage of the proximal phalanx.

their interfaces. The result is a change in the character of the image so that maximum refraction information can be garnered off the peak of the rocking curve, while maximum scatter rejection is achieved at the peak.

Because the attenuation of X-rays is greater in muscle than in fat, even a high-quality conventional radiograph provides distinction between the two tissues (Staren, 1980). DEI, however, provides a higher level of contrast between structures based on scatter rejection, and refraction at the borders between tissues of different densities. It is for this reason that the large tendons, composed of densely packed collagen fibres, could be identified even though they were superimposed by less dense adipose tissue, and muscle in some cases. Indeed, we found that structures, such as articular cartilage and tendons, were best visualized off the peak of the rocking curve where the refraction of X-rays from their outer borders differed from that of the adjacent tissue. Hence, the delineation of tissue structure could be seen wherever a change in refraction existed. A good example of this DEI feature could be found within the fat pad on the plantar side of the foot in which the connective tissue architecture was visualized.

Industrial-grade radiographic film was only used for imaging the articular cartilage of the first metatarsophalangeal joint. Although this film provided high-

er resolution as compared to the image plate, it also required longer imaging times. Thus, a trade-off was necessary to achieve the desired result as the cartilage was very difficult to identify within the joint space using the image plate. However, we are currently applying a CCD camera to the system for digital recordings which will be particularly useful in the eventual computed tomographic application of DEI.

DEI is in its developmental infancy and is currently carried out using a synchrotron. However, the basic principles upon which DEI is based can be extrapolated from the synchrotron and to the clinical setting. In fact, a compact source of X-rays for DEI technology is in the process of being developed (Chapman et al. 1998, and personal communication). Another limitation of DEI in its current form is its projectional viewing perspective. Like conventional radiography, DEI generates two-dimensional images of three-dimensional anatomy. Among other things, this results in superimposition of overlapping structures, which makes interpretation more difficult (Peterfy, 1997). However, DEI computed tomography has already been carried out on simple objects and is currently being developed for complex structures (Chapman et al. 1998, and personal communication). Even in its present form, DEI provides far greater structural information than conventional radiography.

Although conventional radiography is simple, inexpensive and well understood (Dieppe et al. 1992; Peterfy, 1997), further developments of its applications and capabilities in biological imaging were previously thought to be at an impasse. Therefore, any novel application of X-ray imaging, such as presented here, can only stimulate the further development of X-ray technology beyond its current status, particularly in the realm of orthopaedic problems.

Acknowledgments. This work was supported, in part, by NIH grants RO1 AR 48292 and 2-P50-AR 39239 (J.L., A.A., K.K., C.M.) and GM59395-01 (L.C.), DOE grant DE-AC02-98CH10886 (Z.Z.) and in part by a grant from GlaxoSmithKline, Inc.

References

Chapman D, Thomlinson W, Johnston RE, Washburn D, Pisano E, Gmur N, et al. (1997) Diffraction enhanced X-ray imaging. *Phys. Med. Biol.* **42,** 2015-2025.

Chapman LD, Pisano E, Thomlinson W, Zhong Z, Johnston RE, Washburn D, et al. (1998) Medical application of diffraction enhanced imaging. *Breast Dis.* **10,** 197-207.

Dieppe P, Cushnaghan J, McAlindon T (1992) Epidemiology, clinical course, and outcome of knee osteoarthritis. In *Articular Cartilage and Osteoarthritis* (eds Kuettner KE, Schleyerbach R, Peyron JG, Hascall VC), pp. 617-628. New York: Raven Press.

Mollenhauer JA, Aurich ME, Zhong Z, Muehleman C, Cole AA, Hasnah M, et al. (2002) Diffraction-enhanced X-ray imaging of articular cartilage. *Osteoarthritis Cartilage* **10,** 163-171.

Muehleman C, Zhong Z, Williams JM, Kuettner KE, Aurich M, Han B, Mollenhauer J (2002) Diffraction enhanced X-ray imaging of the articular cartilage of experimental animals. *Proceedings of the Ann. Mtg. Orthop. Res. Soc.*, p. 365.

Peterfy C (1997) Imaging techniques. In *Rheumatology* (eds Klippel J, Dieppe P), Vol. 1, p14.1-14.48. Philadelphia: Mosby.

Staren C (1980) The soft tissues. In *A Textbook of Radiology*, 3rd edn (ed. Sutton D), pp. 1025-1048. New York: Churchill Livingstone.

Zachariasen WH (1945) *Theory of X-Ray Diffraction in Crystals.* New York: John Wiley and Sons.

Zhong Z (2000) Using a prism to reject or select harmonic reflections in an X-ray monochromator. *J. Appl. Cryst.* **33,** 1082-1087.

Zhong Z, Thomlinson W, Chapman D, Sayers D (2000) Implementation of diffraction enhanced imaging experiments: at the NSLS and ASP. *Nucl. Instrum. Meth. Phys. Res.* **450,** 556-568.